Preparation and magnetic properties of highly coercive FePt films

T. Shima[a)] and K. Takanashi
Institute for Materials Research, Tohoku University, Sendai 980-8577, Japan

Y. K. Takahashi[b)] and K. Hono
National Institute for Materials Science, 1-2-1 Sengen, Tsukuba 305-0047, Japan

The magnetization processes of highly ordered FePt(001) films with large perpendicular magnetic anisotropy have been studied. The film morphology was controlled from isolated particles to continuous film by varying the nominal thickness (t_N) of the FePt film sputter deposited directly on a MgO(001) substrate at an elevated temperature. A drastic change in the coercivity by one order of magnitude has been found at the critical thickness ($t_N = 45$ nm) where the film morphology changes from a particulate to a continuous state. A huge coercivity exceeding 40 kOe has been achieved in the film with $t_N = 10$ nm, which comprises single domain particles with an average lateral size of approximately 50 nm. © *2002 American Institute of Physics.* [DOI: 10.1063/1.1498504]

Understanding of magnetization processes in magnets of nanometer size is of great technological and scientific interest, because nanoscale patterned or particulate magnets may lead to important applications in various magnetic devices such as high density recording media and bias magnets in monolithic microwave integrated circuits. For these applications, an assembly of nanomagnets with a large uniaxial anisotropy is required. The magnetization processes of fine particles and their assemblies have been extensively investigated for many years.[1–3] The magnetization process, and therefore the coercivity, should depend strongly on the characteristic size and the morphology of materials. However, up to now, little work has been done to correlate experimentally measured magnetization behavior with the actual nanostructural information of ultrathin films.

The $L1_0$ ordered [CuAu (I) type] FePt alloy has attracted much attention in recent years because of the large uniaxial magnetocrystalline anisotropy.[4] The epitaxial growth of FePt films with the *c* axis normal to the film plane was investigated by conventional deposition techniques[5–10] such as sputtering and molecular beam epitaxy (MBE). Much attention has been paid to seek appropriate seed and buffer layers between a single crystalline substrate and FePt thin films,[11,12] in order to control the crystal orientation and the degree of chemical ordering. In most cases, however, the coercivity realized in highly ordered FePt films was less than 20 kOe. The present study demonstrates that extensive variations in the film morphology occur ranging from particulate to continuous states by changing the nominal thickness of the FePt film.

Samples were deposited in a high-vacuum system (base pressure $\sim 5 \times 10^{-10}$ Torr) using multiple dc sputtering with codeposition of Fe and Pt directly onto single crystalline MgO(001) substrates. The targets were commercial products with purities higher than 99.99% at. % for Fe and 99.9 at. % for Pt. High-purity argon of 1.4 mTorr was flown during

sputtering. The substrates were attached to a rotating table, and were heated to 700 °C during the deposition. The nominal thickness of the FePt film (t_N) was varied in the range between 10 and 100 nm. The composition of the films was determined to be $Fe_{52}Pt_{48}$ (at. %) by electron probe x-ray microanalysis (EPMA). The typical growth rate for FePt was 0.12 nm/s.

X-ray diffraction (XRD) with Cu $K\alpha$ radiation was performed for structural characterization. Figure 1 shows a series of XRD patterns for $t_N = 10$ nm (a), 45 nm (b), 50 nm (c), and 100 nm (d). In addition to the fundamental (002) and (004) peaks, (001) and (003) superlattice peaks of the $L1_0$ phase have been clearly observed for all the samples. The unlabeled sharp peaks are due to the MgO substrate. No peaks from the other planes of the $L1_0$ ordered structure are
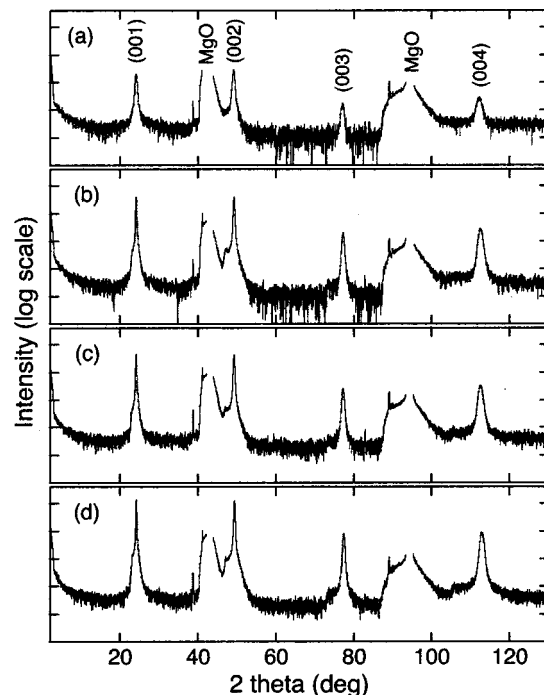
FIG. 1. X-ray diffraction patterns for FePt thin films with different film thicknesses: 10 nm (a), 45 nm (b), 50 nm (c), and 100 nm (d).

[a)]Author to whom correspondence should be addressed; electronic mail: shima@imr.tohoku.ac.jp

[b)]Fellow of Japan Science and Technology Corporation.

Appl. Phys. Lett., Vol. 81, No. 6, 5 August 2002

Shima *et al.*   1051
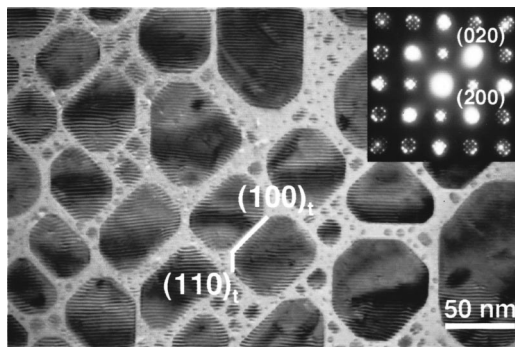
FIG. 2. TEM bright field image and selected area diffraction (SAD) pattern (inset) of FePt thin film with $t_N = 10$ nm thick.

seen because of the strong (001) texture. From the integrated intensities of the fundamental and superlattice peaks extracted from numerical fitting, the degree of long range chemical ordering parameter S was estimated to be 0.95 ± 0.05 for all the films. The detailed procedure for the evaluation has been described elsewhere.[12]

Figure 2 shows a transmission electron microscopy (TEM) image for $t_N = 10$ nm. The films were grown with the island growth mode. Strongly faceted islands of FePt particles are observed with large size distribution. The major facet planes are (100) and (010), and the minor facet plane is (110), indicating that the surface energy of the (100) planes is the lowest. When particles are small, the surface and interfacial energies are large with respect to the volume free energy, and thus small particles would show clear faceting. The stripe contrast observed in the particles are the Moiré pattern originating from the lattice parameter difference between FePt particles and MgO substrates, and their distance is approximately 2.2 nm as expected from the lattice mismatch between FePt and MgO with $a_{FePt} = 0.40$ nm and $a_{MgO} = 0.42$ nm, respectively. The selected area diffraction pattern shows that the orientation relationship (OR) between the FePt particles and the MgO substrate is cube–cube OR, that is $(001)_{FePt} \| (001)_{MgO}$ and $\langle 100 \rangle_{FePt} \| \langle 100 \rangle_{MgO}$. The sizes of the particles are widely distributed with a typical size of about 50 nm per side. In addition, much smaller particles are observed. This suggests that a number of small particles were formed in the initial stage of the film deposition, then they coalesced to form big particles.

A remarkable change in the morphology of the film is observed from the films with different thicknesses, as shown in Fig. 3. With increasing the film thickness, the typical size of particles increases from ~ 50 nm for $t_N = 10$ nm to about 400 nm for $t_N = 20$ nm. With further increase of t_N, particles grow and coalesce, forming an interconnected isotropic maze-like pattern. The maze-like particles do not percolate for $t_N \leqslant 45$ nm. However, the percolation occurs for $t_N = 50$ nm, and the film changes from the discontinuous to continuous morphology. The electron transport measurements also reveal that there is a drastic change in electrical resistance between $t_N = 45$ and 50 nm. The resistances are 800 MΩ and 810 Ω for $t_N = 45$ and 50 nm, respectively. With further increase of t_N, the percolated network expands at the expense of the voids.

Superconducting quantum interference device (SQUID) magnetometry measurements revealed that there is a strong
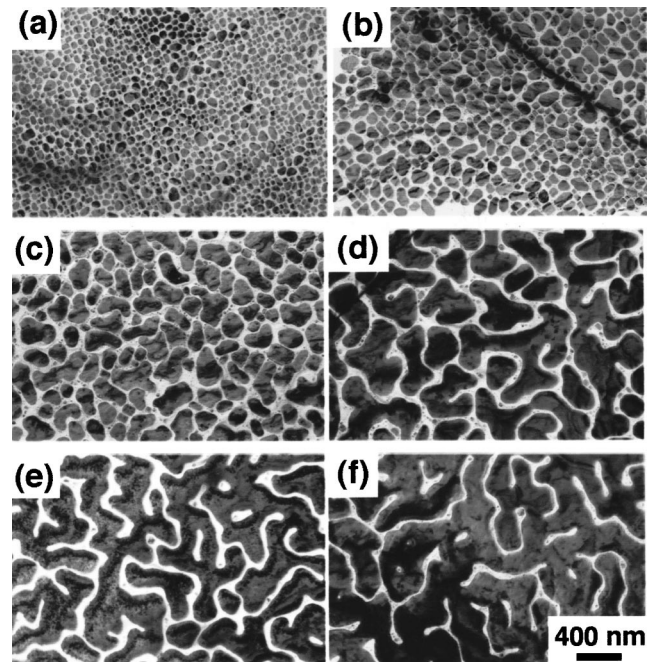
FIG. 3. TEM images of FePt thin films for different film thicknesses: 10 nm (a), 15 nm (b), 20 nm (c), 45 nm (d), 50 nm (e), and 60 nm (f).

t_N dependence of the coercivity (H_c). Figure 4 shows magnetization curves at different film thicknesses. The magnetic easy axis is perpendicular to the film plane for all the samples, since the [001] axis of the tetragonal $L1_0$ ordered structure is perpendicular to the film plane as demonstrated in Fig. 1. Huge H_c of about 40 kOe, which was measured perpendicular to the film plane, was obtained for $t_N = 10$ nm at room temperature. Since the maximum magnetic field of 55 kOe in the SQUID is not sufficient to saturate the magnetization, the real value of H_c and saturation magnetization (M_s) might be even higher. With increasing the film thickness, the coercivity decreases slowly, but still keeps a quite large value of about 25 kOe for $t_N = 45$ nm. However, a drastic change of the magnetization curves is observed between $t_N = 45$ and 50 nm. This critical region corresponds to the change in the morphology of the films from a particulate to a continuous state. With further increase of t_N, the mag-
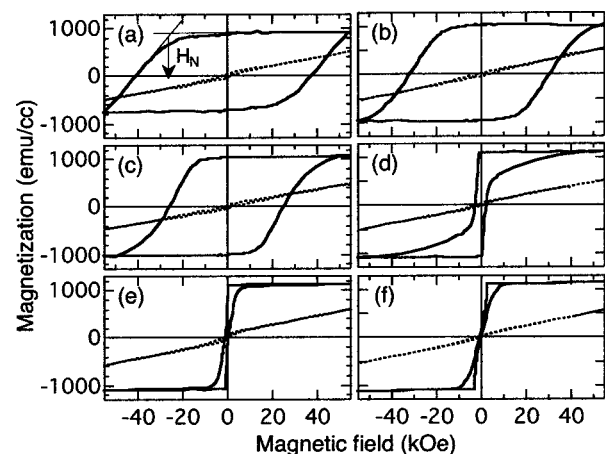
FIG. 4. Magnetization curves for FePt thin films with different film thicknesses: 10 nm (a), 20 nm (b), 45 nm (c), 50 nm (d), 60 nm (e), and 100 nm (f). The magnetic field was applied in the perpendicular direction to the film (solid line) and in the in-plane direction (broken line).
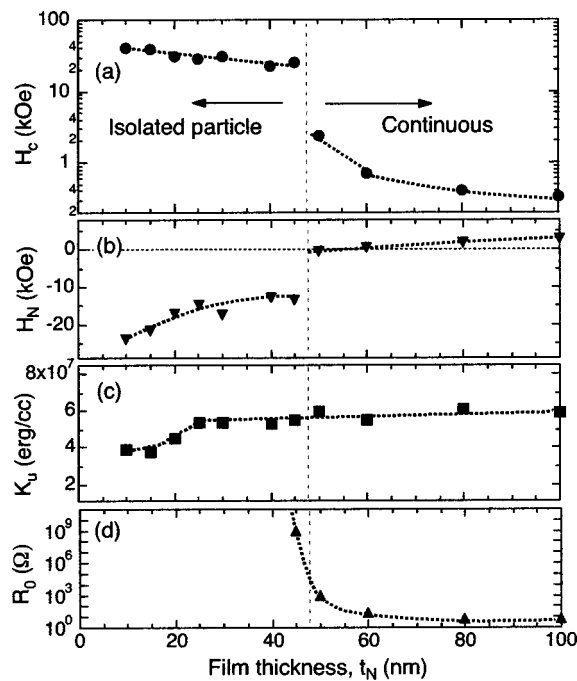
FIG. 5. Magnetic properties and electric resistance for FePt thin films as a function of film thickness t_N. Magnetic properties are coercivity H_c (a), nucleation field H_N (b), and the uniaxial magnetic anisotropy K_u (c), respectively.

netization becomes easier to be saturated for perpendicular direction. In Fig. 5, the magnetic properties and electrical resistance as a function of t_N are summarized. A large coercivity was obtained for $t_N \leq 45$ nm, and a drastic change by one order of magnitude is observed between $t_N = 45$ and 50 nm, as shown in Fig. 5(a). In order to consider the magnetization process, the nucleation field (H_N), at which the magnetization begins to drop with decreasing the field after saturation, is estimated. In the case of the films with large coercivity, the nucleation fields are defined from the cross point of the extrapolation of the values of saturation magnetization and the tangential line at the coercivity. The behavior of H_N is similar to that of coercivity: H_N also changes drastically between $t_N = 45$ and 50 nm. The uniaxial magnetic anisotropy K_u determined from the area enclosed between the magnetization curves in applied fields parallel and perpendicular to the film plane are also shown in Fig. 5(c). The films for $t_N \geq 25$ nm showed a large value of $6.0 \pm 0.5 \times 10^7$ erg/cc, which is very close to the value of fully ordered FePt alloys (7×10^7 erg/cc). Although no jump is seen between $t_N = 45$ and 50 nm, K_u decreases gradually with t_N; this is thought to be attributed to the lack of magnetization saturation associated with the fact that at very small film thicknesses the coercivity in some crystallites is larger than the maximum applied field (55 kOe).

A large distribution in the particle size is observed for $t_N \leq 45$ nm, and the morphology changes from small isolated particles to maze-like discontinuous particles in this region, as shown in Fig. 3. Although the rotation of the magnetization, including an incoherent process such as buckling, is a dominating mechanism in small single-domain particles, the nucleation of domains becomes significant when the particle

size increases,[13] resulting in the decrease of coercivity in this region. When the particles grow and coalesce, percolation occurs for $t_N = 50$ nm. Then, the magnetization process occurs mainly by domain wall displacement and H_c drops dramatically. However, there are still some isolated particles for $t_N = 50$ nm. The magnetization curve characteristic of the coexistence of particles and connected regions is observed for $t_N = 50$ nm. We find two characteristics in the magnetization curve; one is the sudden drop of the magnetization[11,14] at low field ($H_N = -600$ Oe), the other is the high field required to saturate the magnetization. These indicate a low resistance to the movement of the nucleated domain walls within the interconnected regions, and the existence of the particles with much higher nucleation fields. The latter is attributed to the small single domain particles that are present between the interconnected particles. With further increase in t_N, the magnetization becomes easy to be saturated, owing to the disappearance of isolated particles.

This work has clearly demonstrated that a drastic change occurs in the magnetization process of the ordered epitaxially grown FePt films with large perpendicular anisotropy when their morphologies change from particulate to continuous ones. Huge coercivity as high as 40 kOe was obtained from ultrathin films of single domain particulate morphology. This will give fruitful suggestions for not only further theoretical descriptions for actual nanometer scale magnets but also future magnetic applications, such as high-density perpendicular magnetic recording media and artificial patterned media.

[1] C. Kittel, Phys. Rev. **70**, 965 (1946).
[2] E. C. Stoner and E. P. Wohlfarth, Philos. Trans. R. Soc. London, Ser. A **240**, 599 (1948).
[3] J. S. Jacobs and C. P. Bean, Phys. Rev. **100**, 1060 (1995).
[4] O. A. Ovanov, L. V. Solina, and V. A. Demshina, Phys. Met. Metallogr. **35**, 81 (1973).
[5] S. W. Yung, Y. H. Chang, T. J. Lin, and M. P. Hung, J. Magn. Magn. Mater. **116**, 411 (1992).
[6] B. M. Lairson, M. R. Viosokay, R. Sinclair, and B. M. Clemens, Appl. Phys. Lett. **62**, 639 (1993).
[7] B. M. Lairson and B. M. Clemens, Appl. Phys. Lett. **63**, 1438 (1993).
[8] A. Cebollada, D. Weller, J. Sticht, G. R. Harp, R. F. C. Farrow, R. F. Marks, R. Savoy, and J. C. Scott, Phys. Rev. B **50**, 3419 (1994).
[9] M. R. Visokay and R. Sinclair, Appl. Phys. Lett. **66**, 1692 (1995).
[10] M. Watanabe and M. Homma, Jpn. J. Appl. Phys., Part 2 **35**, L1264 (1996).
[11] J.-U. Tiele, L. Folks, M. F. Toney, and D. K. Weller, J. Appl. Phys. **84**, 5686 (1998).
[12] T. Shima, T. Moriguchi, S. Mitani, and K. Takanashi, Appl. Phys. Lett. **80**, 288 (2002).
[13] C. Kittel, Rev. Mod. Phys. **21**, 541 (1949).
[14] C. Kooy, U. Enz, Philips Res. Rep. **15**, 7 (1960).